Significant Pressure-Induced Enhancement of Optoelectronic Properties in WS_2 Nanotubes

JIANG Yifeng[1], YUE Lei[1,*], WEI Ziyu[2], ZHAO Xiaoxu[3], LI Quanjun[1,*], LIU Bingbing[1]

1. State Key Laboratory of High Pressure and Superhard Materials, Jilin University, Changchun 130012, China
2. College of Physical Science and Technology, Heilongjiang University, Harbin 150080, China
3. School of Materials Science and Engineering, Peking University, Beijing 100871, China

Abstract

Exploring effective approaches to optimize the optoelectronic properties of functional materials is crucial for the development of next-generation optoelectronic devices. However, existing tuning strategies often involve complex fabrication processes, and the intrinsic relationship between structural evolution and optoelectronic enhancement in one-dimensional transition metal dichalcogenides (TMDs) under extreme conditions remains unclear, limiting further improvements in performance. In this study, pressure tuning was used to significantly enhance the optoelectronic response of WS_2 nanotubes (NT-WS_2). At 13.5 GPa, the device responsivity increased to 43.75 A W^{-1}, nearly two orders of magnitude higher than its initial value, while the external quantum efficiency increased by approximately 67-fold, respectively. In situ high-pressure X-ray diffraction and Raman spectroscopy show that the enhanced optoelectronic performance of NT-WS_2 arises from band-gap narrowing caused by strengthened interlayer interactions under pressure, together with improved carrier transport resulting from the dense packing of the nanotubes. This work not only advances the understanding of the optoelectronic evolution of one-dimensional TMDs under extreme conditions, but also provides new insights into the design and optimization of high performance nanoscale optoelectronic devices.

Keywords: High pressure; Transition metal dichalcogenides; Nanotubes; Optoelectronic response;

PACS: 07.35.+k,61.46.Fg,73.63.-b

The paper is an English translated version of the original Chinese paper published in Acta Physica Sinica. Please cite the paper as: JIANG Yifeng, YUE Lei, WEI Ziyu, ZHAO Xiaoxu, LI Quanjun, LIU Bingbing **Significant Pressure-Induced Enhancement of Optoelectronic Properties in WS_2 Nanotubes**. *Acta Phys. Sin.*, 2026, 75(3): 030803 DOI: 10.7498/aps.75.20251345

DOI: 10.7498/aps.75.20251345

CSTR: 32037.14.aps.75.20251345

1 Introduction

Among low-dimensional materials, one-dimensional (1D) nanomaterials show great promise for high-speed transport, low energy consumption, and highly sensitive detection because of their unique geometries and quantum confinement effects. Since the controlled synthesis of WS_2 nanotubes (NT-WS_2) was achieved in 1992, they have attracted widespread attention [1]. In addition to their applications in tribology and composite reinforcement [2–4], the potential of NT-WS_2 for photodetection and optoelectronic devices has gradually become apparent. Previous studies have shown that photodetectors based on individual NT-WS_2 can achieve high sensitivity and broadband response [5,6], highlighting their unique advantages in nano-optoelectronics. However, the key to fully exploiting the potential of such low-dimensional materials lies in effectively tuning their optoelectronic properties. The crystal structure and electronic band structure of a material largely determine its optoelectronic properties [7], and rational tuning of the band-gap structure and optical transition mechanisms is therefore essential for achieving excellent performance. Although conventional approaches, such as constructing heterojunctions [8–10] and elemental doping [11,12], can improve photoelectric conversion efficiency, they often introduce impurities and complex interfaces, thereby obscuring the intrinsic structure–property relationship of the material. Therefore, there is an urgent need to explore clean, efficient, and controllable physical methods to reveal the evolution of electronic structures in low dimensional semiconductors and enable precise optimization of their optoelectronic performance.

High pressure is a “clean” and efficient external stimulus that can continuously and reversibly tune the crystal structure, electronic band structure, and optical transition processes without introducing impurities [13–16], thereby enabling significant improvements in performance. In recent years, important progress has been made in the high pressure-tuning of transition metal dichalcogenides [17–22], perovskites [23–26], and other low dimensional materials [27], including band-gap tuning, increased carrier concentrations, and extension of the spectral response. Our previous work showed that applied pressure enhanced the photocurrent of two-dimensional layered WS_2 by nearly 30-fold and extended its photoresponse range to 1450 nm, highlighting the unique advantages of high pressure for tuning the optoelectronic properties of low-dimensional semiconductors [28]. On this basis, the present study extends the pressure-tuning strategy to one-dimensional WS_2 nanotubes, systematically investigates their

optoelectronic response under high pressure, and examines the influence of morphological dimensionality on the tuning behavior. The experimental results show that the photocurrent of NT-WS_2 is enhanced by up to 84-fold at 13.5 GPa. Combined analysis of the in situ high-pressure X-ray diffraction and Raman spectroscopy results reveals that this pronounced enhancement mainly originates from pressure-induced band-gap narrowing and the close packing between the nanotube walls. This study not only deepens the understanding of the optoelectronic evolution of one-dimensional TMDs under extreme conditions, but also provides new insights into the design and optimization of high-performance nano-optoelectronic devices.

2 Experimental Methods

2.1 Sample Preparation

The WS_2 nanotubes were synthesized using a top-down solid-state reaction method [29]. The samples used in this study were provided by the research groups of Prof. Reshef Tenne at the Weizmann Institute of Science, Israel, and Prof. Alla Zak at the Holon Institute of Technology.

2.2 Ambient Pressure Characterization

The sample morphology was examined using an FEI Magellan 400 field-emission scanning electron microscope (SEM), and the microstructure was analyzed by transmission electron microscopy (TEM) and high-resolution transmission electron microscopy (HRTEM) using a JEM-2200FS microscope. X-ray diffraction (XRD) and Raman spectroscopy were also used to characterize the structural features of the samples.

2.3 High-Pressure Measurements

High-pressure XRD and Raman measurements: Diamond anvils with culet diameters of 400 μm were used in the experiments. The gasket was pre-indented and then drilled to form a hole with a diameter of 180 μm. Pressure was calibrated using the ruby fluorescence peak shift method. High-pressure Raman measurements were performed using a Horiba Raman spectrometer with a 532 nm diode-pumped solid-state (DPSS) green laser as the excitation source. High-pressure XRD measurements were carried out using Mo Kα radiation (λ = 0.7107 Å) on the same Rigaku Synergy Custom FR-X instrument used for the ambient-pressure measurements.

High-pressure optoelectronic measurements: A symmetric diamond anvil cell (DAC) equipped with diamond anvils having culet diameters of 400 μm was used to generate high pressure. A steel gasket was first pre-indented and drilled. Epoxy resin

was applied to the gasket surface, and cubic boron nitride (c-BN) was packed into the hole to insulate the gasket from the electrical leads. The gasket was then re-drilled to form a sample chamber with a diameter of 250 μm. Electrical measurements were performed in a two-probe configuration, with two platinum (Pt) electrodes placed parallel to each other and in contact with the sample surface. No pressure-transmitting medium was used throughout the measurements. A xenon lamp was used as the light source, and optical filters were used to obtain incident light at specific wavelengths. The optical power was measured using a CEL-NP2000 laser power meter, and the measurement configuration is shown in Fig. S1. Because drift in the power-meter reading may introduce small errors, the average of multiple repeated measurements was taken as the incident power. The photocurrent was measured using a Keithley 2461 source-measure unit at a sampling rate of 5 Hz.

3 Results and Discussion

3.1 Material Characterization

The NT-WS_2 nanotubes used in the experiments were first systematically characterized at ambient pressure. Figure 1(a) shows a transmission electron microscopy (TEM) image of the nanotubes, revealing a hollow, multiwalled structure with lengths of several micrometers. Figure 1(c) presents the energy dispersive X-ray spectroscopy (EDS) spectrum of NT-WS_2 together with the corresponding elemental maps, clearly showing that the constituent elements W and S are uniformly distributed throughout the sample. The high-resolution TEM image reveals a multilayer stacking structure, with a spacing of 0.63 nm between adjacent layers, slightly larger than the interlayer spacing of bulk WS_2 reported in the literature [30]. This larger spacing is mainly attributed to local strain near the curved regions of the nanotubes. In regions with less pronounced curvature or relatively flat surfaces, the interlayer spacing decreases but remains larger than that of the bulk material. At the local scale, each layer resembles the typical structure of monolayer WS_2 : each W atom is surrounded by six S atoms in a trigonal prismatic configuration. Previous studies have also shown that the layers of multiwalled nanotubes have different chiralities. An individual multiwalled nanotube device typically consists of zigzag, armchair, and chiral single-walled nanotubes. Similar to boron nitride nanotubes, their point groups are C_2 nh, C_2 nv, and Cn, respectively. Therefore, zigzag and chiral single-walled nanotubes are intrinsically polar and non-centrosymmetric, providing favorable conditions for their pronounced bulk photovoltaic effect [31]. Nevertheless, the overall diffraction characteristics of the nanotubes remain highly similar to those of bulk 2H-WS_2 . Notably, the slight shifts of the (002), (004), and (006) diffraction peaks in Fig. 1(e)

are consistent with the high resolution TEM results, further indicating that the interlayer spacing of the nanotubes is slightly larger than that of the bulk material and reflecting the effects of curvature and local strain on the lattice. Ambient pressure Raman measurements were also performed on NT-WS_2 , as shown in Fig. 1(f). Three Raman vibrational modes were observed: the in-plane E_2 g 1 mode at 352 cm^{-1}; involving opposite in-plane shear motions of the W and S atoms; the interlayer A_1 g mode at 421 cm^{-1}; involving synchronous stretching motions of adjacent layers along the c axis; and the "silent" B_1 u mode at 416 cm^{-1}; involving opposite stretching motions of adjacent layers along the c axis. The B_1 u mode is weak in bulk materials but is significantly enhanced in nanomaterials because of structural disorder. It is a characteristic mode for distinguishing nanotubes from the bulk phase [32], in agreement with previous results [33].

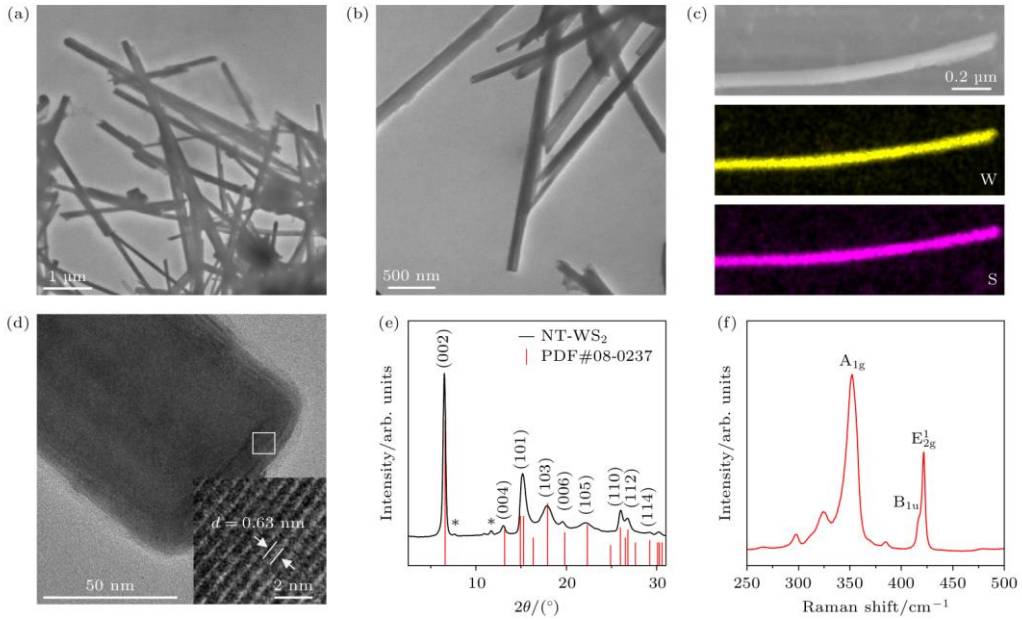

Fig. 1. (a), (b) TEM images of NT-WS_2; (c) SEM image and EDS elemental maps of NT-WS_2; (d) HRTEM image of NT-WS_2; (e) ambient-pressure XRD pattern of NT-WS_2, with the red vertical lines indicating the diffraction-peak positions of bulk WS_2 from the standard Powder Diffraction File (PDF) card. The peaks marked with asterisks correspond to the unconverted WO_x phase formed during synthesis, possibly $W_{18}O_{49}$ or WO_2; (f) ambient-pressure Raman spectrum of NT-WS_2.

3.2 High-Pressure Optoelectronic Properties of NT-WS_2

The evolution of the optoelectronic properties of NT-WS_2 under high pressure was systematically investigated by in situ high-pressure photoresponse measurements using a two-electrode method. During the measurements, a xenon lamp was used as the light source, and the light spot was larger than the sample to ensure uniform illumination of the sample. The incident light power density was maintained at 1.6

mW cm^{-2}, and the bias voltage was fixed at 0.1 V throughout the experiment. Figure 2(a) presents the time-dependent photoresponse at selected pressures. NT-WS_2 exhibited a clear photoresponse over the entire experimental pressure range. At the initial pressure, the photocurrent was approximately 416 nA. As pressure increased, the photocurrent increased continuously and reached 34.98 μA at the highest experimental pressure of 13.5 GPa, representing an approximately 84-fold increase over the initial value. This increase is significantly greater than the pressure-induced enhancement observed in bulk 2H-WS_2 [28], indicating the unique potential of one-dimensional nanotubes for optoelectronic tuning under high pressure. The photoresponse characteristics were further quantified by calculating the photocurrent density J□ □ and responsivity R using the following equations:

$$J_{\mathrm{ph}} = \frac{I_{\mathrm{ph}}}{S}, \qquad (1)$$

$$R = I_{\mathrm{ph}}/(P_{\mathrm{in}}S), \qquad (2)$$

Here, the net photocurrent is defined as I□ □ = I$_{light}$ − I$_{dark}$, where I$_{light}$ and I$_{dark}$ represent the output currents under illumination and in the dark, respectively. S is the effective irradiation area of 5×10^{-4} cm^2, and P$_{in}$ is the incident light power density of 1.6 mW cm^{-2}. At the initial pressure, J□ □ and R were 0.80 mA cm^{-2} and 0.50 A W^{-1}, respectively. As pressure increased, both the photocurrent density and responsivity increased continuously. At 13.5 GPa, J□ □ reached 70 mA cm^{-2} and R reached 43.75 A W^{-1}. Compared with the optoelectronic performance of bulk WS_2 under pressure (5 V, 20.1 GPa, 692.9 A W^{-1}) [28], NT-WS_2 exhibited an excellent response at a lower bias voltage and lower pressure (0.1 V, 13.5 GPa, 43.75 A W^{-1}), highlighting its combined advantages in terms of energy consumption and sensitivity. Notably, the photocurrent response speed of NT-WS_2 was relatively slow, as shown in Fig. S2. This may be related to the tendency of nanomaterials to form defects. Defects can prolong the carrier lifetime and thereby enhance photoconductive gain, but this occurs at the expense of response speed [34]. In addition, to evaluate the contact between the electrodes and NT-WS_2, we measured the dark I–V curves, as shown in Fig. 2(d). The current–voltage relationship was linear, indicating that good Ohmic contact was formed between NT-WS_2 and the Pt electrodes. This linear relationship remained unchanged throughout compression, excluding the influence of contact resistance on the photoresponse and confirming that the pressure-dependent photocurrent originated from the intrinsic properties of NT-WS_2. The resistance values obtained by fitting the I–V curves showed that the resistance of NT-WS_2 decreased rapidly with increasing pressure. At 13.5 GPa, the resistance decreased by approximately two orders of magnitude compared with its initial value. In addition, the photoresponse of NT-WS_2 after decompression to 0.8 GPa was compared with

that measured at 0.9 GPa during compression, as shown in Fig. S3. The results indicate that the photoresponse was reversible after decompression and showed good recoverability.

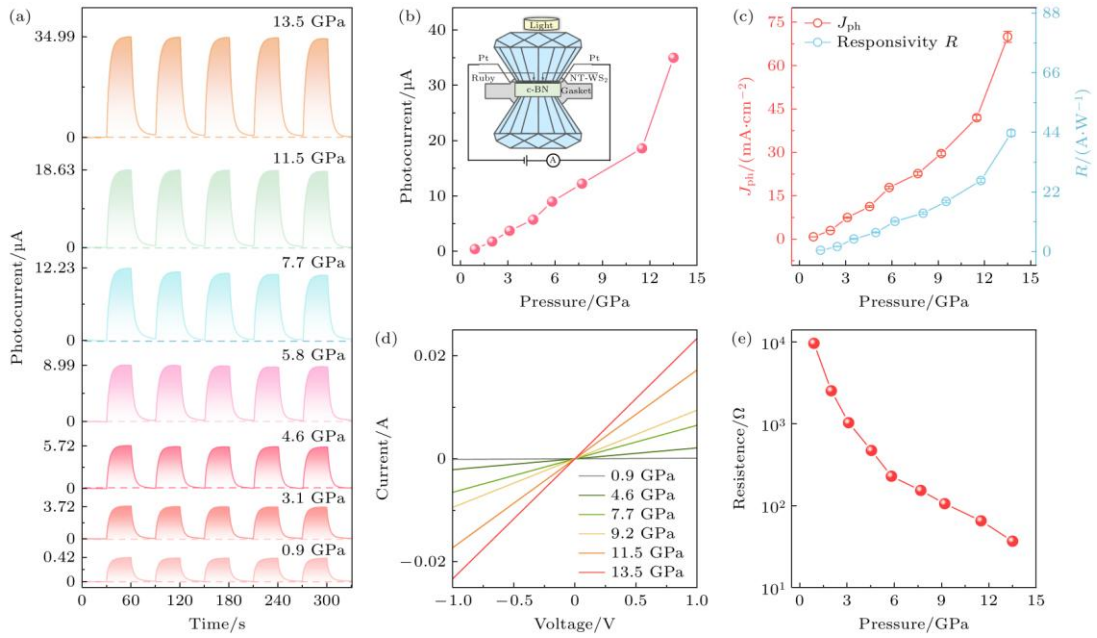

Fig. 2. Evolution of the optoelectronic properties of NT-WS_2 under xenon lamp illumination at a bias voltage of 0.1 V during compression to 13.5 GPa: (a) photoresponse at different pressures; (b) photocurrent of NT-WS_2, with the inset showing a schematic of the experimental setup; (c) photocurrent density and responsivity; (d) I–V characteristic curves; and (e) resistance variation.

The contribution of incident light at different wavelengths to the photocurrent was further evaluated by measuring the photoresponse under visible light illumination at 400, 500, 600, and 650 nm. Figure 3(a) shows the photocurrent curves obtained under illumination at these wavelengths during compression. The results show that, at the same pressure, illumination at 500 nm produced the largest photocurrent. When the pressure increased to 13.5 GPa, the photocurrents at all wavelengths increased by tens of times compared with those at the initial pressure, consistent with the trend observed under full-spectrum illumination. External quantum efficiency (EQE) and specific detectivity D* are also key parameters for characterizing optoelectronic performance and were calculated using the following equations:

$$\mathrm{EQE} = R\frac{hc}{e\lambda}, \qquad (3)$$

$$D^* = R\sqrt{\frac{S}{2eI_d}}, \qquad (4)$$

where I_d is the dark current, h is Planck's constant (6.626×10^{-34} J s), c is the speed of light (3×10^8 m s^{-1}), e is the elementary charge (1.6×10^{-19} C), and λ is the

corresponding wavelength. The calculation results show that, with increasing pressure, both the external quantum efficiency and responsivity of the NT-WS_2 photoresponse increased rapidly, with an enhancement of approximately 67-fold. As a key indicator of photodetector sensitivity, the specific detectivity D* showed a steady increase over the pressure range of 0.9–13.5 GPa, rising from an initial value of 3.24×10^9 Jones to 1.25×10^{10} Jones. These results show that pressure not only significantly enhanced the photoresponsivity of WS_2 nanotubes, but also improved their photoelectric conversion efficiency and device sensitivity. Therefore, high pressure can significantly enhance the optoelectronic performance of NT-WS_2, fully demonstrating the excellent optoelectronic tunability of one-dimensional nanotubes under extreme conditions.

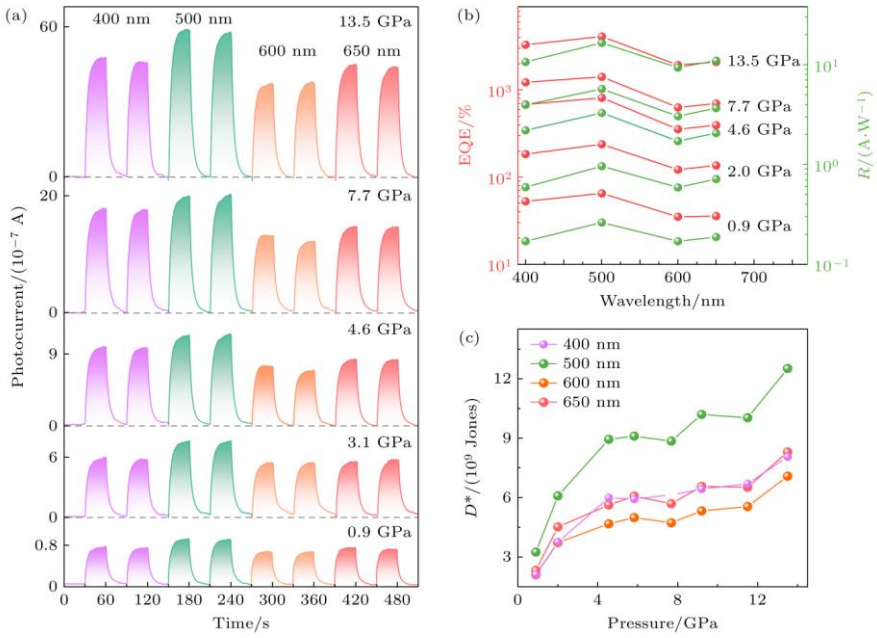

Fig. 3. (a) Photocurrent response of NT-WS_2 under illumination at 400, 500, 600, and 650 nm at selected pressures; (b), (c) variations in the external quantum efficiency, responsivity, and specific detectivity of NT-WS_2 with pressure.

3.3 High-Pressure Structure of NT-WS_2

Pressure-induced structural evolution in NT-WS_2 was examined by high-pressure X-ray diffraction (XRD) measurements over the pressure range of 0–15.5 GPa, as shown in Fig. 4(a). With increasing pressure, all diffraction peaks shifted collectively toward higher angles, indicating compression of the unit cell. Meanwhile, some diffraction peaks broadened and decreased in intensity, reflecting pressure-induced lattice distortion in the nanotubes. No new diffraction peaks were observed within the experimental pressure range, indicating the absence of a structural phase transition. After decompression, the XRD pattern recovered to its initial state,

demonstrating that the structural evolution of NT-WS_2 is reversible within the studied pressure range. The pressure dependence of the lattice parameters and unit-cell volume was further determined by Rietveld refinement of the XRD data using GSAS, as shown in Figs. 4(b)–4(d). The results show that the compressibility along the c axis is significantly higher than that along the a axis under pressure. At 15.5 GPa, the c axis and a axis are shortened by approximately 12% and 4%, respectively. This anisotropic compression behavior can be directly attributed to the crystal structure characteristics of NT-WS_2 , in which atoms within the layers are bonded by strong covalent bonds, whereas adjacent layers are held together by weak van der Waals interactions.

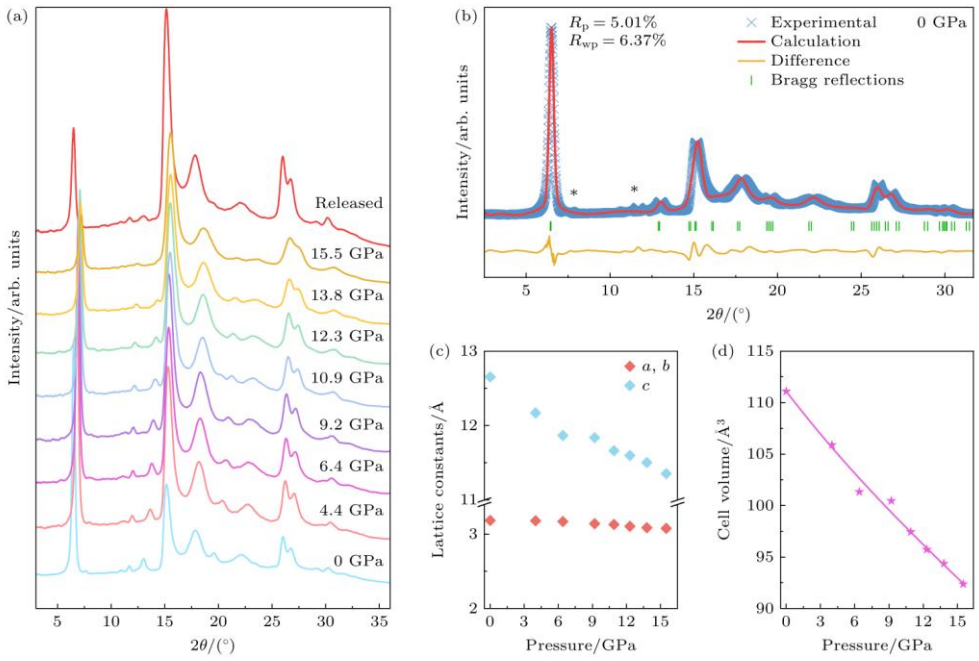

Fig. 4. (a) High-pressure XRD patterns of NT-WS_2 over the pressure range up to 15.5 GPa; (b) ambient-pressure XRD Rietveld refinement pattern of NT-WS_2; (c), (d) variations in the lattice parameters a, b, and c and unit-cell volume V of NT-WS_2 with pressure.

The role of pressure in enhancing the optoelectronic properties of NT-WS_2 was further investigated by in situ Raman spectroscopy over the pressure range of 1.1–15.8 GPa, as shown in Fig. 5(a). The three characteristic vibrational modes, E_2 g, B_1 u, and A_1 g, all exhibited continuous hardening with increasing pressure, as shown in Fig. 5(b), and no new peaks appeared, further confirming the absence of a structural phase transition. This result is consistent with previous measurements performed using silicone oil as the pressure-transmitting medium, indicating that the pressure environment does not change the phase transition pathway [35]. Notably, after decompression from 15.8 GPa to ambient pressure, the Raman spectrum fully recovered its initial profile, indicating that the structural changes during compression are reversible. This phenomenon is consistent with the higher compressibility along

the c axis revealed by the high-pressure XRD analysis, and together these results confirm the significant enhancement of interlayer S–S atomic interactions during compression. Quantitative analysis shows that the pressure coefficients of the E_2 g, B_1 u, and A_1 g modes are 1.47, 1.37, and 2.73 $cm^{-1}GPa^{-1}$, respectively. The hardening trends of these three modes indicate that both the intralayer and interlayer interactions in NT-WS_2 are enhanced under pressure, while the much larger pressure coefficient of the A_1 g mode highlights its particularly high sensitivity to pressure.

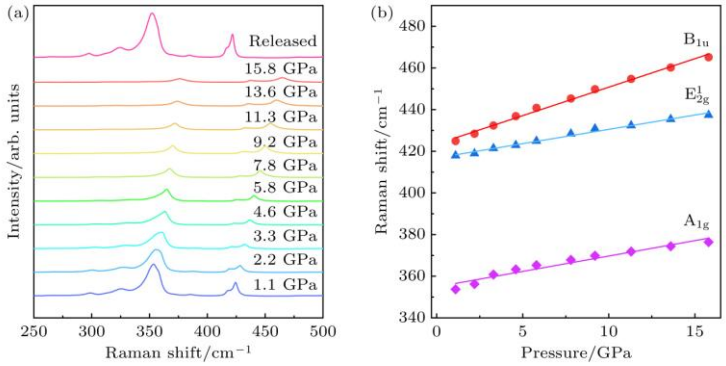

Fig. 5. High-pressure Raman characterization of NT-WS_2 under 532 nm laser excitation: (a) high-pressure Raman spectra; (b) evolution of the Raman vibrational modes with pressure.

Previous theoretical studies have shown that, in two-dimensional layered WS_2, pressure-induced shortening of the interlayer spacing enhances interlayer interactions and strengthens the coupling between W 5d and S 3p orbitals, leading to increased dispersion of the valence and conduction bands and, consequently, continuous band-gap narrowing [28]. Similarly, the reduced interlayer spacing in NT-WS_2 under pressure can also lead to band-gap narrowing, lower the energy barrier for electronic transitions, promote photoexcitation of valence-band electrons, and generate a large number of electron–hole pairs, thereby significantly enhancing its photoresponse. Notably, compared with bulk WS_2, in which the c axis contracts by approximately 11% and the a axis by approximately 4% at 21.8 GPa, NT-WS_2 exhibits stronger pressure sensitivity. This difference in structural response provides a reasonable physical explanation for its performance enhancement compared with bulk materials. In addition, nanotubes that are loosely distributed at low pressure gradually become closely packed during compression [36], thereby forming more efficient charge-transport channels and significantly improving carrier transport. Overall, the synergistic effect of band-gap narrowing and improved carrier transport drives the pronounced enhancement of the photoresponse of NT-WS_2 under pressure, providing an important foundation for its application in high-performance optoelectronic devices.

4 Conclusion

Pressure tuning significantly enhanced the photoresponse of WS_2 nanotubes. At 13.5 GPa, the device responsivity increased by nearly two orders of magnitude, while the external quantum efficiency increased by approximately 67-fold, respectively. These enhancements far exceed those observed in bulk WS_2 , highlighting the unique advantages of one-dimensional nanostructures for performance tuning. High-pressure XRD and Raman spectroscopy analyses indicate that this pronounced enhancement mainly arises from pressure-induced band-gap narrowing associated with strengthened interlayer interactions, together with efficient carrier transport between the nanotubes. The results further reveal the structure–property relationship of NT-WS_2 under high pressure and provide new insights into the functional tuning of low-dimensional transitionmetal dichalcogenides and the design of high-performance optoelectronic devices.

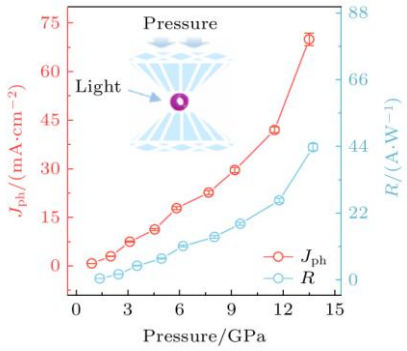

References

[1] Tenne R, Margulis L, Genut M E, Hodes G 1992 *Nature* **360** 444

[2] Rapoport L, Bilik Y, Feldman Y, Homyonfer M, Cohen S, Tenne R 1997 *Nature* **387** 791

[3] Kaplan-Ashiri I 2004 AIP Conf. Proc. 723 306

[4] Wang M S, Kaplan-Ashiri I, Wei X L, Rosentsveig R, Wagner H D, Tenne R, Peng L M 2008 *Nano Res.* **1** 22

[5] Pelella A, Kumar A, Intonti K, Durante O, De Stefano S, Han X, Li Z, Guo Y, Giubileo F, Camilli L, Passacantando M, Zak A, Di Bartolomeo A 2024 *Small* **20** 2403965

[6] Wang F C, Wei S J, Jin W Y, He X L, Wang W F, Wang F J, Li F, Zhang X Y, An Q W, He X B, Xu J P 2025 *J. Phys. D: Appl. Phys.* **58** 195103

[7] Wu X Q, Wang L R, Yuan Y F, Ma L, Guo H Z 2023 *Chin. J. High Press. Phys.* **37** 050103

[8] Zhang Y J, Onga M, Qin F, Shi W, Zak A, Tenne R, Smet J, Iwasa Y 2018 *2D Mater.* **5** 035002

[9] Faella E, Lozzi L, Camilli L, Zak A, Giubileo F, Bartolomeo A D, Passacantando M 2025 *Nanotechnology* **36** 325501

[10] Li C K, Zhu J L 2025 *Acta Phys. Sin.* **74** 176802

[11] Xia H, Lu Z Y, Li T X, Parkinson P, Liao Z M, Liu F H, Lu W, Hu W D, Chen P P, Xu H Y 2012 ACS Nano 6 6005

[12] Gao L F, Wang L D, Kuklin A V, Gao J, Yin S C, Ågren H, Zhang H 2021 *Small* **17** 2105683

[13] Li Z L, Li H Y, Liu N N, Du M Y, Jin X L, Li Q J, Du Y, Guo L, Liu B B 2021 *Adv. Opt. Mater.* **9** 2101163

[14] Li Z L, Jia B X, Fang S X, Li Q J, Tian F Y, Li H Y, Liu R, Liu Y C, Zhang L J, Liu S Z, Liu B B 2022 *Adv. Sci.* **10** 2205837

[15] Li Z L, Li Q J, Li H Y, Tian F Y, Du M Y, Fang S X, Liu R, Zhang L J, Liu B B 2022 *Small Methods* **6** 2201044

[16] Yue L, Tian F Y, Liu R, Li Z L, Li R X, Li C Y, Li Y C, Yang D L, Li X D, Li Q J, Zhang L J, Liu B B 2025 *Natl. Sci. Rev.* **12** nwae419

[17] Zhang X T, Liu B, Liu S, Li J Y, Liu R, Wang P, Dong Q, Li S J, Tian H, Li Q J, Liu B B 2021 *J. Alloys Compd.* **867** 158923

[18] Chen S X, Li Z L, Li S C, Xu K B, Ma N, Yue L, Jin X L, Liu R, Dong Q, Li Q J, Liu B B 2025 *Laser Photonics Rev.* **19** 2500250

[19] Yan X L, Feng Z B, Yu L, Liu C L 2025 *Acta Phys. Sin.* **74** 177801

[20] Chi Z H, Zhao X M, Zhang H D, Goncharov A F, Lobanov S S, Kagayama T, Sakata M, Chen X J 2014 *Phys. Rev. Lett.* **113** 036802

[21] Ma X L, Fu S H, Ding J W, Liu M, Bian A, Hong F, Sun J T, Zhang X X, Yu X H, He D W 2021 *Nano Lett.* **21** 8035

[22] Wang P, Wang Y G, Qu J Y, Zhu Q, Yang W G, Zhu J L, Wang L P, Zhang W W, He D W, Zhao Y S 2018 *Phys. Rev. B* **97** 235202

[23] L ü X J, Wang Y G, Stoumpos C C, Hu Q Y, Guo X F, Chen H J, Yang L X, Smith J S, Yang W G, Zhao Y S, Xu H W, Kanatzidis M G, Jia Q X 2016 *Adv. Mater.* **28** 8663

[24] Zhang J K, Ji S H, Ma Y Z, Guan R Q, Wu X X, Qu X, Yan B M, Zhang D Z, Zhao J L, Yang J H 2019 *Nanoscale* **11** 11660

[25] Guo S H, Bu K J, Li J W, Hu Q Y, Luo H, He Y H, Wu Y H, Zhang D Z, Zhao Y S, Yang W G, Kanatzidis M G, L ü X J 2021 *J. Am. Chem. Soc.* **143** 2545

[26] Wu S Y, Ma S L, Zhao C Y, Li S X, Ye M Y, Qi M Y, Zhao X B, Wang L R, Cui T 2025 *Acta Phys. Sin.* **74** 178503

[27] Liu T B, Bu K J, Zhang Q, Zhang P J, Guo S H, Liang J Y, Wang B H, Zheng H Y, Wang Y G, Yang W G, L ü X J 2022 *Materials* **15** 3845

[28] Zhang X T, Dong Q, Li Z L, Jing X L, Liu R, Liu B, Zhao T T, Lin T, Li Q J, Liu B B 2022 *Mater. Res. Lett.* **10** 547

[29] Zak A, Sallacan-Ecker L, Margolin A, Feldman Y, Popovitz-Biro R, Albu-Yaron A, Genut M, Tenne R 2010 *Fuller. Nanotub. Carbon Nanostruct.* **19** 18

[30] Bandaru N, Kumar R S, Baker J, Tschauner O, Hartmann T, Zhao Y, Venkat R 2014 *Int. J. Mod. Phys. B* **28** 1450168

[31] Zhang Y J, Ideue T, Onga M, Qin F, Suzuki R, Zak A, Tenne R, Smet J H, Iwasa Y 2019 *Nature* **570** 349

[32] Krause M, Virsek M, Remškar M, Kolitsch A, Möller W 2009 Phys. Status Solidi (b) 246 2786

[33] Staiger M, Rafailov P, Gartsman K, Telg H, Krause M, Radovsky G, Zak A, Thomsen C 2012 *Phys. Rev. B* **86** 165423

[34] Yue L, Cui D D, Tian F B, Liu S, Li Z L, Liu R, Yao Z, Li Y C, Yang D L, Li X D, Li Q J, Du Y, Liu B B 2024 *Acta Mater.* **263** 119529

[35] Yue L, Xu D, Wei Z Y, Zhao T T, Lin T, Tenne R, Zak A, Li Q J, Liu B B 2022 *Materials* **15** 2838

[36] O'Neal K R, Cherian J G, Zak A, Tenne R, Liu Z, Musfeldt J L 2016 *Nano Lett.* **16** 993